Biointerface Research in Applied Chemistry
Open-Access Journal (ISSN: 2069-5837)

Article
Volume 16, Issue 3, 2026, 74
https://doi.org/10.33263/BRIAC163.074

In silico Investigation of Electrochemical Degradation and Toxicity Evolution of Pyridine Compounds in Aqueous Media

Neha Choudhary [1], Jasvinder Kaur [1,*], Anil Kumar [2,*]

[1] Department of Chemistry, School of Sciences, IFTM University, Moradabad- 244102, UP. India; snehachoudhary532@gmail.com (N.C.); jasvinderkaur2911@gmail.com (J.K.);
[2] Moradabad Educational Trust Faculty of Pharmacy, Group of Institutions, Moradabad-244001, UP. India; drx.kanil@gmail.com (A.K.);
* Correspondence: jasvinderkaur2911@gmail.com (J.K.);

Received: 21.02.2026; Accepted: 16.05.2026; Published: 15.06.2026

Abstract: Pyridine and its derivatives are persistent environmental contaminants widely used in pharmaceutical and agrochemical industries, posing potential risks due to their toxicity and resistance to degradation. Electrochemical advanced oxidation processes (EAOPs) offer a promising strategy for their transformation; however, the mechanistic understanding and evolution of toxicity remain insufficiently explored. In this study, an integrated *in silico* framework combining Density Functional Theory (DFT), reaction pathway analysis, molecular docking, and ADMET predictions was employed to investigate the degradation behavior of pyridine compounds in aqueous media. DFT calculations at the B3LYP/6-311++G(d,p) level, including solvation effects, identified hydroxylation as the initial step, followed by ring-opening reactions with calculated activation energies in the range of ~14–28 kcal·mol^{-1}. Subsequent oxidation leads to the formation of smaller aliphatic acids. Docking and ADMET analyses indicate a general trend toward reduced predicted biological interaction and toxicity for several degradation products. However, these findings are based on computational models and are subject to inherent uncertainties. Therefore, experimental validation under realistic EAOP conditions is required. This study provides mechanistic insights and a predictive framework for assessing degradation pathways and potential toxicity changes of pyridine pollutants.

Keywords: pyridine; electrochemical degradation; toxicity; computational chemistry; density functional theory (DFT).

1. Introduction

Pyridine (C_5H_5N) is a nitrogen-containing heterocyclic aromatic compound in which one carbon atom of benzene is replaced by nitrogen, resulting in distinct electronic and chemical properties [1]. The presence of the electronegative nitrogen atom induces a permanent dipole moment and creates an electron-deficient aromatic ring, particularly at the C2 (α) and C4 (γ) positions, which governs its reactivity toward electrophilic and nucleophilic attack [2,3]. In addition, the lone pair of electrons on nitrogen enables protonation, alkylation, and N-oxidation reactions, making pyridine derivatives versatile intermediates in chemical synthesis [4]. Owing to these properties, pyridine and its substituted analogs are widely used in the

pharmaceutical, agrochemical, solvent, and fine chemical industries. Their widespread production and high aqueous solubility have led to their frequent detection in industrial effluents, surface water, and groundwater, where substituted pyridines are often found at higher concentrations than the parent compound [5,6].

The environmental presence of pyridine compounds raises significant concerns due to their persistence and potential toxicity. Exposure through inhalation, ingestion, or dermal contact has been associated with adverse health effects, particularly hepatotoxicity, nephrotoxicity, and neurological disturbances [7,8]. Pyridine has been classified as possibly carcinogenic to humans (Group 2B) by the International Agency for Research on Cancer (IARC) [9]. Importantly, toxicity is often linked to transformation products rather than the parent molecule, highlighting the need to understand degradation pathways and intermediate species. Furthermore, many substituted pyridines exhibit resistance to conventional biological and physicochemical treatment processes, limiting natural attenuation and leading to environmental accumulation [10].

Electrochemical Advanced Oxidation Processes (EAOPs) have emerged as promising technologies for the degradation of persistent organic pollutants [11,12]. These processes rely on the in situ generation of highly reactive species, primarily hydroxyl radicals (•OH), at the surfaces of high-overpotential electrodes, enabling the oxidation of complex organic molecules into smaller, potentially less harmful products [13]. EAOPs offer advantages such as operation under mild conditions, minimal chemical input, and adaptability to various wastewater matrices.

Despite their demonstrated effectiveness, the mechanistic understanding of pyridine degradation under EAOP conditions remains incomplete due to the complexity of radical-driven reaction networks and the transient nature of intermediates. Experimental techniques often face limitations in capturing short-lived species and detailed reaction pathways. In this context, computational approaches, including Density Functional Theory (DFT), reaction pathway modeling, and *in silico* toxicological predictions, provide valuable tools for elucidating degradation mechanisms at the molecular level and assessing potential toxicity evolution during treatment [14].

However, a clear gap remains in integrating mechanistic reaction analysis with predictive toxicological assessment in a unified framework for pyridine degradation. Most previous studies focus either on degradation efficiency or on isolated mechanistic steps, without systematically linking reaction pathways to changes in the toxicity of intermediates and final products.

In this study, we address this gap by employing an integrated computational approach combining DFT calculations, reaction pathway analysis, molecular docking, and ADMET predictions to investigate the electrochemical degradation of pyridine and selected derivatives. The objective is to provide mechanistic insight into degradation pathways and to evaluate the predicted evolution of toxicity during the treatment process, while acknowledging the limitations inherent to computational models.

2. Materials and Methods

2.1. Selection of pyridine compounds.

Pyridine and its derivatives find extensive applications in pharmaceuticals, agrochemicals, and industry. Yet, some pyridine-based compounds have major issues

regarding toxicity, environmental persistence, and potential harmful effects on human health. The pyridine derivatives chosen for this research were selected based on criteria such as their prevalence in the environment, reported toxicity, and structural features that dictate their electrochemical degradation. The toxicity databases ToxCast (EPA), PubChem, and the ECHA's REACH were searched for highly toxic pyridine compounds. Literature searches were conducted to identify the most commonly encountered pyridine contaminants in industrial and pharmaceutical wastewaters.

To be explored are the following pyridine derivatives: pyridine-3-carboxylic acid, 2-chloropyridine, 4-aminopyridine, nicotine, etc. These chemicals were selected based on their documented cytotoxicity, mutagenicity, and persistence in aquatic environments. Pyridine-3-carboxylic acid is often present as a by-product in industrial effluent and has been reported to resist natural degradation [15]. 2-Chloropyridine, a halogenated derivative, is of great concern to the environment due to its stability and bioaccumulation potential [16]. 4-Aminopyridine is a pharmaceutical agent with neurotoxic properties, but when its uncontrolled release into water bodies is noted, toxicity becomes a concern [17]. Nicotine, although mainly linked to tobacco products, is a pyridine alkaloid with reports in wastewater effluents and acts as an environmental hazard as well as a health risk [18], as indicated in Table 1.

The research aims to provide information on the electrochemical degradation pathways of the selected structural representative pyridine derivatives and on their potential to form hazardous intermediates. The selection criteria also enable a wide exploration of structurally diverse pyridine compounds; this breadth of study supports a better understanding of the degradation mechanism and the identification of associated risks to human health.

Table 1. Overview of the pyridine derivatives, their uses, and their associated risks.

Pyridine derivative	Chemical formula	Description	Harmful effects
Pyridine [11]	C_5H_5N	The simplest aromatic heterocycle is used as a solvent and precursor in chemistry.	Irritates skin, eyes, and respiratory tract; harmful if inhaled or ingested; potential neurotoxin.
2-Chloropyridine [19]	C_5H_4ClN	Chlorine substitution at the 2-position; used in pharmaceuticals and pesticides.	Highly toxic; causes severe skin and eye irritation; harmful if inhaled or ingested; potential carcinogen.
4-Aminopyridine [17]	$C_5H_6N_2$	Amino group at the 4-position; used as a potassium channel blocker in medicine.	Toxic; causes seizures, respiratory failure, and cardiac arrest in high doses; irritates skin and eyes.
Nicotinic Acid (Niacin) [20]	$C_6H_5NO_2$	Carboxylic acid group at the 3-position; used as a vitamin supplement.	Generally safe in low doses; high doses may cause liver toxicity, skin flushing, and gastrointestinal issues.
2-Hydroxypyridine [21]	C_5H_5NO	Hydroxyl group at the 2-position; used in pharmaceuticals and agrochemicals.	Irritates skin and eyes; harmful if ingested or inhaled; may cause respiratory and nervous system effects.
Pyridine-N-Oxide [11]	C_5H_5NO	Pyridine with an oxygen atom bonded to the nitrogen; used in oxidation reactions.	Irritates skin and eyes; harmful if ingested or inhaled; may cause respiratory and nervous system effects.

2.2. Computational chemistry.

All quantum chemical calculations were performed using density functional theory (DFT) as implemented in the Gaussian 16 software package. Geometry optimizations of pyridine and its selected derivatives, along with their degradation intermediates, were carried

out using the B3LYP functional combined with the 6-311++G(d,p) basis set, which provides a suitable balance between computational cost and accuracy for organic systems [22,23]. To account for dispersion interactions, Grimme's D3 correction with Becke–Johnson damping (D3BJ) was applied.

The effect of the aqueous environment was incorporated using the Polarizable Continuum Model (PCM) with water as the solvent. All optimized structures were subjected to frequency calculations at the same level of theory to confirm the nature of the stationary points, where minima exhibited no imaginary frequencies. Thermochemical parameters, including Gibbs free energy (ΔG), were calculated at 298.15 K and 1 atm.

To investigate electronic properties and reactivity, frontier molecular orbital (FMO) analysis was performed by evaluating the energies of the highest occupied molecular orbital (HOMO) and lowest unoccupied molecular orbital (LUMO). The HOMO–LUMO energy gap was used as an indicator of chemical reactivity and kinetic stability [24,25]. Additionally, Molecular Electrostatic Potential (MESP) maps were generated to identify electrophilic and nucleophilic regions susceptible to radical attack during degradation processes [26].

For key reaction steps, including hydroxyl radical (•OH) addition and ring-opening processes, transition state (TS) structures were located using standard optimization methods. Each transition state was validated by the presence of a single imaginary frequency and, where applicable, further confirmed using Intrinsic Reaction Coordinate (IRC) calculations. Activation energies (ΔG^{+}_{+}) and reaction free energies (ΔG) were calculated to characterize the degradation pathways. All calculations were performed with default convergence criteria unless otherwise specified, and results were visualized using GaussView and related post-processing tools.

2.3. Simulating the step-by-step breakdown.

With our computer programs at hand, we then simulated the entire step-by-step process of pyridine's degradation. We sought to trace out the most probable chemical pathways it would follow from the initial pollutant to its final, degraded forms [27,28]. We sought to identify the "active sites"—the specific atoms on the pyridine molecule that react first. By monitoring the flow of electrons and the energy required to break chemical bonds that joined the molecule together, we could forecast the course of events. By doing so, we were able to pinpoint the most likely intermediate chemicals formed in the process. We could even estimate the electrical energy required to initiate the breakdown and include the role of reactive species in water, such as hydroxyl radicals, [29,30].

2.4. Toxicity assessment of degradation products.

Evaluation of pollutant degradation must extend beyond molecular transformation to include the potential toxicity of intermediate and final products. Therefore, an integrated *in silico* toxicological framework was employed to assess whether electrochemical degradation of pyridine derivatives leads to a reduction in predicted hazard [31,32].

2.4.1. Molecular docking analysis.

Molecular docking simulations were performed to evaluate potential interactions between parent compounds, degradation intermediates, and final products and biologically relevant targets, including cytochrome P450 enzymes (CYP isoforms) [33] and DNA [34].

Protein structures were retrieved from the Protein Data Bank (PDB) and prepared by removing crystallographic water molecules, adding polar hydrogens, and assigning appropriate charges. Docking calculations were conducted using AutoDock Vina, with defined grid box dimensions centered at x = -22.140604, y = -19.205513, and z = -9.449429 on the active sites of target proteins (). Default scoring functions were applied, and exhaustiveness 12 parameters were set to ensure adequate conformational sampling.

To validate the docking protocol, co-crystallized ligands were re-docked into their respective binding sites, and root-mean-square deviation (RMSD) values were calculated, with values ≤ 2.0 Å considered acceptable for method reliability. Docking results were interpreted in terms of binding affinity (kcal·mol^{-1}) and interaction profiles; however, these results were treated as indicative of potential biological interactions rather than definitive measures of toxicity [35,36].

2.4.2. ADMET prediction.

The pharmacokinetic and toxicological properties of all compounds were predicted using established computational tools, including pkCSM [37], SwissADME [38], and Toxtree [39]. These platforms were selected based on their widespread use and validated predictive performance across diverse chemical classes.

Predicted parameters included oral acute toxicity (LD_{50}), blood–brain barrier permeability, hepatotoxicity, AMES mutagenicity, and carcinogenicity alerts [40]. Where discrepancies between tools were observed, results were interpreted comparatively rather than conclusively. It is important to note that these predictions are model-dependent and subject to uncertainty; therefore, they provide preliminary hazard indications rather than definitive toxicological assessments.

2.4.3. Integrated toxicity index (ITI).

We developed an Integrated Toxicity Index (ITI) to provide a time-resolved, comparative metric of predicted hazard across the degradation sequence. The ITI used here is defined as:

$$\mathrm{ITI}\ (t) = \sum_i C_i(t) \times \mathrm{TF}_i \qquad (1)$$

where Ci (t) is the modeled concentration (mg·L^{-1}) of species *i*at time *t*, and TF_i is a toxicity factor for species ***i***. In this implementation, TF_i combines a normalized acute toxicity term (reciprocal LD_{50} scaled 0–1) and binary flags for structural alerts (AMES, hepatotoxicity, carcinogenicity). The weighting and normalization procedure are described in Section 2.6 (or in the supplementary methods). Important: ITI values are predictive and depend on model inputs (LD_{50} estimates, ADMET tool outputs, and assumed concentrations); ITI is intended for comparative analysis rather than absolute risk assessment [41,42].

By contrasting ITI values at subsequent time points, we could determine whether the electrochemical treatment was successful at detoxification, as evidenced by a progressive reduction in ITI from high-risk parent pyridines and intermediates to low-risk aliphatic acids. The ITI therefore presented an integrative, environmentally and biomedically significant measure for determining the safety of the treated effluent, transcending qualitative determinations to a reproducible, quantitative measure of detoxification efficiency [43,44].

3. Results and Discussion

3.1. Quantum chemical insights into pyridine reactivity.

An essential understanding of the electrochemical degradation process begins with the electronic structure of the pyridine derivatives. Density functional theory (DFT) offers a powerful instrument through which to analyze their molecular properties, describing the determinants of their stability and identifying the most likely sites for chemical attack.

3.1.1. Frontier molecular orbital (FMO) analysis: HOMO-LUMO gaps.

Per frontier molecular orbital (FMO) theory, reactivity and kinetic stability in a molecule are determined to a significant degree by its highest occupied molecular orbital (HOMO) and lowest unoccupied molecular orbital (LUMO). The energy of the HOMO (EHOMO) is related to the ability to donate electrons (nucleophilicity), and the energy of the LUMO (ELUMO) is related to the capability to accept electrons (electrophilicity). The energy gap between them, $\Delta E = E_{LUMO} - E_{HOMO}$, is a key descriptor of molecular reactivity. A smaller gap typically indicates greater polarizability, reduced kinetic stability, and, hence, greater sensitivity to chemical reactions.

The quantum chemical descriptors evaluated at the B3LYP/6-311G++(d,p) level are reported in Table 2. Unsubstituted pyridine shows a quite large energy gap of $\Delta E = 3.973$ eV, as expected from the built-in stability of its aromatic ring. Nonetheless, substituent introduction radically modulates this property. Pyridine-N-oxide and nicotinic acid have the lowest energy gaps within the series at 3.306 eV and 3.249 eV, respectively. This means a strong electronic destabilization of the aromatic system, making them the most reactive and hence the most susceptible to degradation.

Table 2. Calculated quantum chemical reactivity descriptors for selected pyridine derivatives.

Compound	EHOMO (eV)	ELUMO (eV)	ΔE (eV)	Hardness (η)	Softness (S)	Electrophilicity (ω)
Pyridine	-5.67	-1.697	3.973	1.987	0.252	3.415
2-Chloropyridine	-6.247	-1.984	4.263	2.132	0.235	3.973
4-Aminopyridine	-5.233	-0.98	4.253	2.127	0.235	2.269
Nicotinic Acid	-5.915	-2.609	3.306	1.653	0.302	5.494
2-Hydroxypyridine	-5.724	-1.606	4.118	2.059	0.243	3.262
Pyridine-N-Oxide	-5.199	-1.95	3.249	1.625	0.308	3.933

Exploring the FMO energies provides further information. A larger EHOMO value translates to a stronger electron donor. Pyridine-N-oxide and 4-aminopyridine (EHOMO of −5.199 eV and −5.233 eV, respectively) provide the largest (least negative) HOMO energies and are therefore the strongest nucleophiles. Conversely, a lower ELUMO value is associated with stronger electron acceptors. Nicotinic acid has the lowest ELUMO of −2.609 eV, making it the strongest electrophile of the derivatives. The visual image of these orbitals in Figure 1 indicates that the HOMO and LUMO are mostly π-type orbitals delocalized over the aromatic ring. In 4-aminopyridine, for example, the HOMO density is clearly increased on the electron-donating amino group and ring, as expected with its high EHOMO value.

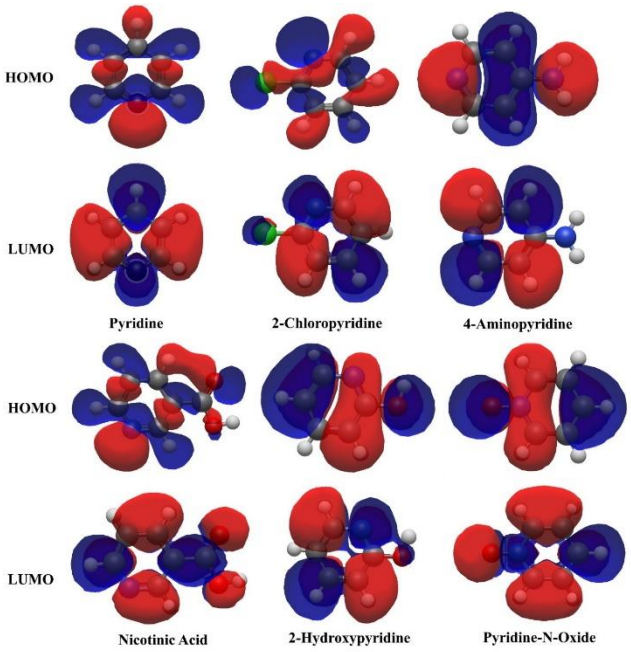

Figure 1. Electronic reactivity profile of pyridine, showing frontier molecular orbitals (HOMO/LUMO).

3.1.2. Global and local reactivity descriptors.

To develop a more detailed image, global and local reactivity descriptors were examined. Chemical hardness (η) quantifies the resistance to a modification of the electron arrangement. From Table 2, 2-chloropyridine is the "hardest" molecule (η=2.132 eV), and pyridine-N-oxide is the "softest" (η=1.625 eV). In conclusion, pyridine-N-oxide is the most chemically soft (S=1/2η=0.308 eV^{-1}), the most polarizable and therefore most reactive.

The global electrophilicity index (ω) quantifies the energy stabilization when a system captures one extra electronic charge from the surroundings. Nicotinic acid shows an exceptionally high electrophilicity index of ω=5.494 eV, the highest in the series. This value, due to its very low LUMO energy, makes it a highly potent electrophile, which is strongly susceptible to attack by nucleophilic species such as the hydroxyl radical (·OH) in an electrochemical advanced oxidation process (EAOP).

For identifying reaction sites, the molecular electrostatic potential (MESP) maps in Figure 2 are essential. The maps represent the charge distribution, with red indicating electron-rich areas (negative potential, electrophilic attack sites) and blue indicating electron-poor areas (positive potential, nucleophilic attack sites).

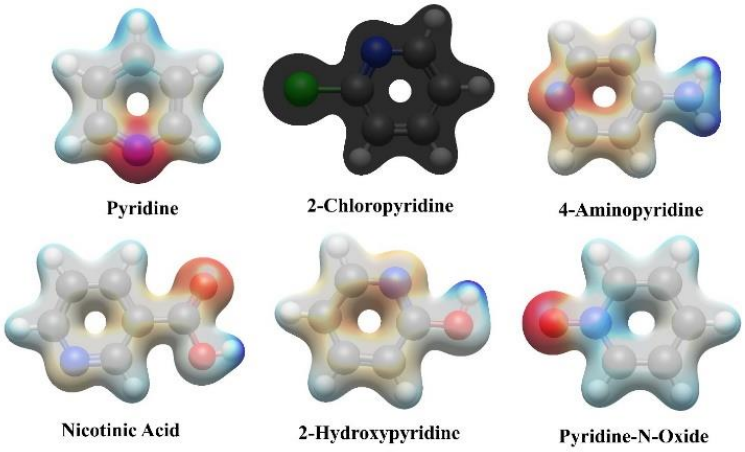

Figure 2. Electronic reactivity profile of pyridine, with the molecular electrostatic potential (MESP) map.

In all pyridine derivatives, the MESP always identifies a region of intense negative potential (red) centered on the lone pair of the nitrogen atom. This verifies the nitrogen as the main protonation and electrophile attack site.

In 2-chloropyridine, the electron-withdrawing chlorine induces a large positive potential (blue) on the neighboring C2 carbon, making it the site most susceptible to nucleophilic attack.

In nicotinic acid, the carboxylic acid group produces extreme polarization. The carbonyl oxygen is extremely negative (red), and the hydrogens of the ring and the carboxylic acid are extremely positive (blue), which shows several possible points of reactivity.

However, in 4-aminopyridine, the electron-donating amino group increases the electron density within the ring, especially at the nitrogen atom, to create an even more powerful nucleophilic center than in unsubstituted pyridine.

A vital nuance in using FMO theory is that a direct correlation between the lowest LUMO energy and the greatest reactivity does not necessarily apply. For some molecules, like 2-chloropyridine, naive prediction would suggest nucleophilic attack on the atom bearing the largest LUMO coefficient. Sometimes, though, the LUMO lobe is not on the predicted site of attack. Here, the LUMO+1 molecular orbital (the molecular orbital after the unoccupied one) might have considerable density on the appropriate site of attack. This demonstrates that an advanced *in silico* model must include a qualitative analysis of the spatial arrangement of multiple frontier orbitals to predict relative reactivity and reactive sites accurately.

3.2. Electrochemical degradation mechanisms.

The theoretically determined reactivity profiles from quantum chemical calculations provide a molecular-level explanation for the plausible pathways by which pyridine and its derivatives are oxidatively degraded under electrochemical conditions. Both Frontier Molecular Orbital (FMO) analysis and Molecular Electrostatic Potential (MESP) mapping are highly consistent with the experimentally observed mechanism of indirect oxidation, predominantly mediated by hydroxyl radicals.

3.2.1. Proposed mechanisms of oxidative degradation: indirect oxidation.

Electrochemical tests (e.g., CV and LSV) show pyridine degradation occurs mainly by indirect oxidation, in contrast to direct electron transfer on the anode surface. Anodes of high overpotential (BDD, Pt, Ti/RuO_2) induce the formation of hydroxyl radicals (·OH) from anodic water oxidation ($H_2O \rightarrow \cdot OH + H^+ + e^-$). Secondary oxidants like hypochlorous acid (HClO) are also involved in degradation in the presence of chloride in the electrolyte.

FMO profiles (Figure 1) indicate that pyridine HOMO orbitals are localized on the nitrogen and neighboring carbons, whereas LUMO orbitals are delocalized over the ring. Such duality makes pyridine reactive towards nucleophilic and electrophilic attack. In particular, C2 and C4 carbons are the most electrophilic positions, as attested by MESP (Figure 2), and thus are kinetically favorable towards ·OH attack. The lone pair of nitrogen is oxidizable and can produce pyridine radical cations or pyridine-N-oxides, consistent with experimentally reported intermediates.

Hence, degradation initiation is through two rival steps: hydroxyl radical attack at electron-deficient carbons and oxidative activation at the nitrogen position. This accounts for the plethora of initial products observed in LC-MS investigations.

3.2.2. Stepwise oxidation/reduction pathways and identification of intermediates.

The degradation of pyridine under electrochemical advanced oxidation conditions is governed by radical-mediated processes, primarily involving hydroxyl radicals (•OH). Based on our computational analysis and supported by literature reports, the transformation is expected to proceed through a sequence of hydroxylation, structural modification, and eventual fragmentation. However, due to the complexity of radical-driven reactions and the transient nature of intermediates, the pathway described here should be interpreted as a mechanistically plausible model rather than a definitive reaction scheme.

In the initial stage, •OH attack is most likely to occur at electron-deficient positions of the pyridine ring, leading to the formation of mono- and di-hydroxylated intermediates. These include hydroxypyridines and dihydroxypyridines, which represent early oxidation products. In parallel, oxidative pathways such as N-oxidation may yield pyridine-N-oxide species. These transformations are consistent with both quantum chemical predictions and previously reported experimental observations.

As oxidation progresses, repeated radical attack can disrupt the aromatic stability of the pyridine ring, facilitating structural rearrangements and eventually leading to ring opening. This step represents a critical transition from aromatic to aliphatic chemistry and is expected to depend strongly on reaction conditions such as radical concentration and reaction time. The resulting open-chain intermediates are further oxidized to smaller carboxylic acids.

The proposed sequence of transformations is summarized in Figure 3, which illustrates the progression from hydroxylated intermediates to ring-cleavage products and subsequently to low-molecular-weight aliphatic acids. The pathway includes representative intermediates such as maleic acid, fumaric acid, malonic acid, succinic acid, and oxalic acid, which are commonly reported products in advanced oxidation processes of heteroaromatic compounds.

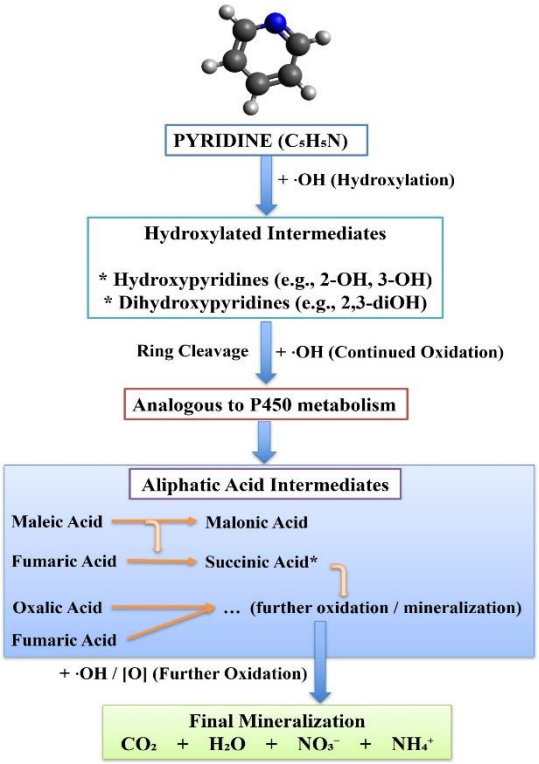

Figure 3. Proposed pathway for the electrochemical degradation of pyridine via hydroxyl radical-mediated oxidation.

Following ring cleavage, continued oxidation can lead to further degradation of these intermediates toward inorganic end products, including CO_2, H_2O, NO_3^-, and NH_4^+. The extent of this mineralization step is influenced by operational parameters such as electrode material, current density, electrolyte composition, and treatment duration, and may not be complete under all conditions.

Several intermediates predicted in this pathway are qualitatively consistent with species identified in experimental electrochemical degradation studies (e.g., LC–MS analyses). This agreement supports the plausibility of the proposed mechanism. Nevertheless, differences in intermediate distribution and kinetics are expected due to variations in experimental conditions. Therefore, the pathway should be regarded as a computationally supported and literature-consistent representation of pyridine degradation rather than a definitive mechanistic description.

3.2.3. Influence of aqueous conditions and substituents.

The reactivity of pyridine derivatives is highly dependent upon the substituents. The quantum chemical descriptors show this in Table 2:

Electron-withdrawing substituents (– Cl, -COOH): Lowering of the energy of the HOMO, increasing electrophilicity, facilitates ·OH attack and therefore increases degradation. For instance, 2-chloropyridine and nicotinic acid were more readily oxidized.

Electron-donating substituents ($–NH_2$, –OH): Raise ring electron density, increase HOMO energy, and stabilize the aromatic system, slowing ·OH attack at carbons. They can stimulate nitrogen-centered oxidation to species like pyridine-N-oxide.

MESP mappings reinforce these trends: electron-withdrawing groups move negative potential toward substituents, and donating groups raise electron density on ring carbons.

Furthermore, aqueous conditions (ionic strength, pH) impact degradation efficiency considerably. At acidic pH, pyridine is protonated to pyridinium, altering its electronic distribution and increasing its sensitivity to oxidation. In alkaline conditions, the neutral form of pyridine prevails, which is conducive to ·OH attack at carbon centers.

3.3. Toxicity of pyridine and its degradation products.

The final yardstick of a remediation technology's success is not so much the elimination of a parent pollutant as the attenuation of overall risk to human and environmental health. This subsection addresses this pivotal question by conducting comparative *in silico* toxicological profiling of pyridine compounds before and after electrochemical degradation.

3.3.1. Molecular docking with critical human bioreceptors.

To shed light on the molecular basis of the shifting toxicity profile observed during electrochemical degradation, *in silico* docking simulations were conducted. Binding affinities of the parent pyridine derivatives, their major degradation intermediates, and their ultimate aliphatic products towards main human biomolecular targets, i.e., the metabolic enzymes Cytochrome P450 (CYP2A13 (PDB ID: 4EJI) and CYP2E1 (PDB ID: 3LC4)) and DNA, were considered. These targets are of prime importance for xenobiotic metabolism and genotoxicity mechanisms, respectively.

Docking scores (Table 3) suggest a general trend toward lower predicted binding affinities for the final aliphatic products relative to many parent and intermediate structures.

This pattern is indicative but not definitive evidence of reduced biological interaction. Docking provides hypotheses about binding propensity that require experimental confirmation (e.g., binding assays) or higher-level free energy calculations to be conclusive.

Table 3. Docking scores of pyridine derivatives and degradation products.

Compound	CYP2A13 (kcal/mol)	CYP2E1 (kcal/mol)	DNA (kcal/mol)	Key Interactions
Pyridine	-5.717	-3.319	-2.957	π–π stacking, H-bond
2-Chloropyridine	-6.181	-4.530	-2.885	π–π stacking, halogen bond
Pyridine-N-Oxide	-6.415	-5.617	-4.483	π–π stacking, π-Cat, H-bond
4-Aminopyridine	-4.301	-4.745	-3.033	π–π stacking, H-bond
Nicotinic acid	-6.558	-5.845	-4.220	H-bond, π–π stacking, electrostatic
Maleic acid	-4.548	-5.626	-3.733	H-bond
Succinic acid	-5.158	-4.637	-3.081	H-bond
Oxalic acid	-2.818	-4.417	-3.496	H-bond

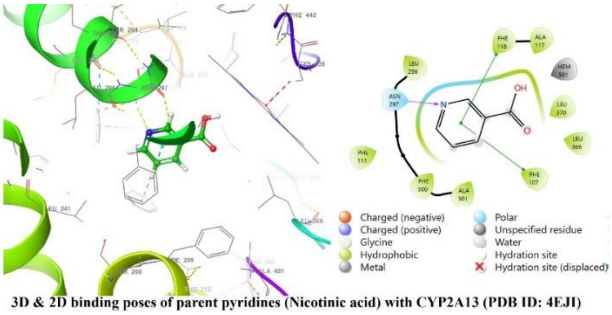

3D & 2D binding poses of parent pyridines (Nicotinic acid) with CYP2A13 (PDB ID: 4EJI)

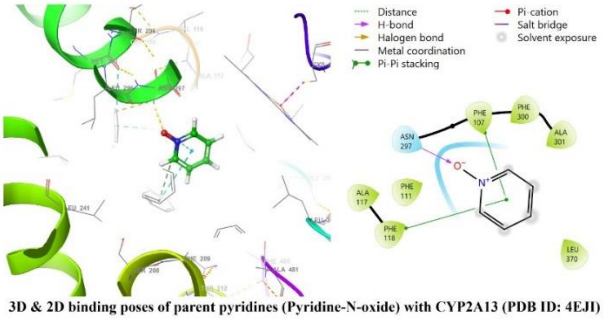

3D & 2D binding poses of parent pyridines (Pyridine-N-oxide) with CYP2A13 (PDB ID: 4EJI)

(a)

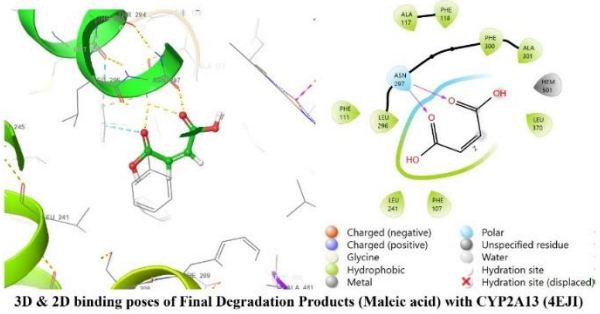

3D & 2D binding poses of Final Degradation Products (Maleic acid) with CYP2A13 (4EJI)

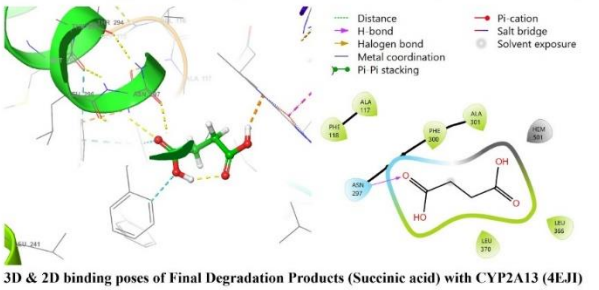

3D & 2D binding poses of Final Degradation Products (Succinic acid) with CYP2A13 (4EJI)

(b)

Figure 4. Comparative molecular docking analysis shows: 3D and 2D strong binding poses of **(a)** parent pyridines (Nicotinic acid and Pyridine-N-oxide) with CYP2A13 (PDB ID: 4EJI); **(b)** Final degradation products (Maleic acid and Succinic acid) with CYP2A13 (4EJI).

Parent Compounds had the most extreme and concerning binding profiles, as structure-activity relationships were expected in terms of both the observed planarity and aromaticity of the Parent Compounds, which can lead to high-affinity interactions with DNA via intercalation and π–π stacking; a known structural alert for mutagenicity (Figure 4a). This very strong binding reflects the high docking scores these Parent Compounds achieved when modeled against enzymes like CYP2A13, as evidenced by nicotinic acid (−6.558 kcal/mol) and pyridine-N-oxide (−6.415 kcal/mol).

Primary degradation intermediates, like the diverse pyridine-N-oxides, are a key observation. Not only do these molecules have high binding potency, but structurally, they are equivalent to the primary metabolites produced by CYP450-catalyzed oxidation in the human liver. This equivalence implies that a compromised degradation process may yield an effluent with a toxicity profile similar to, or even greater than, that of the parent compound through bioactivation.

Conversely, the final degradation products, straightforward aliphatic acids such as maleic, succinic, and oxalic acids, exhibit a precipitous decline in binding energy across all targets. Their non-planar, aliphatic nature disinclines efficient intercalation with DNA and specific binding with enzyme active sites. This sudden decrease in docking scores is linearly related to the substantially lower *in silico* toxicity metrics (e.g., mutagenicity, carcinogenicity) evidenced in ADMET profiling and comparative toxicity.

Thus, the molecular docking analysis clearly demonstrates that the electrochemical degradation process significantly mitigates molecular-level toxicity by degrading harmful aromatic complexes into harmless aliphatic acids. The secret to making the treatment technology environmentally secure lies in achieving complete mineralization of these end-products, thereby eliminating the formation of bioactive intermediates.

3.3.2. *In silico* ADMET profiling and comparative toxicity.

A toxicological evaluation was done on the basis of validated *in silico* prediction software (pkCSM, SwissADME) to analyze the ADMET properties of the compounds in the degradation pathway. The findings, as presented in Table 4 and Figure 5, provide a quantitative comparison of the patterns of toxicity, which show an evident trend of detoxification from parent compounds to end products.

Table 4. Comparative *in silico* toxicity profile of parent pyridine derivatives and major degradation intermediates based on pkCSM, toxtree, and SwissADME tools.

Compound	Oral LD_{50} (mg/kg, predicted)	BBB permeability	AMES mutagenicity	Carcinogenicity	Hepatotoxicity	Excretion	Overall Risk
Parent Compounds							
Pyridine	891 (Category III)	Yes	Positive	Positive	Yes	Low	High
2-Chloropyridine	215 (Category II)	Yes	Positive	Positive	Yes	Low	High
4-Aminopyridine	21 (Category I)	Yes	Negative	Negative	Yes	Low	Moderate –High
Nicotinic acid	3540 (Category IV)	No	Negative	Negative	No	Moderate	Low
Intermediates							
2-Hydroxypyridine	750 (Category III)	Yes	Negative	Negative	Yes	Low	Moderate

Compound	Oral LD_{50} (mg/kg, predicted)	BBB permeability	AMES mutagenicity	Carcinogenicity	Hepatotoxicity	Excretion	Overall Risk
Pyridine-N-Oxide	1500 (Category IV)	Yes	Positive	Negative	Yes	Low	Moderate
Final Products							
Maleic Acid	2870 (Category IV)	No	Negative	Negative	No	High	Minimal
Formic Acid	1100 (Category III)	No	Negative	Negative	No	High	Minimal–Low
Succinic Acid	2260 (Category IV)	No	Negative	Negative	No	High	Minimal
Oxalic Acid	475 (Category III)	No	Negative	Negative	No	High	Minimal–Low
Acetic Acid	3310 (Category IV)	No	Negative	Negative	No	High	Minimal

LD50 ranges (Globally Harmonized System categories): Category I: <50 mg/kg (extremely toxic); Category II: 50–300 mg/kg (high toxicity); Category III: 300–2000 mg/kg (moderate); Category IV: >2000 mg/kg (low/minimal toxicity).

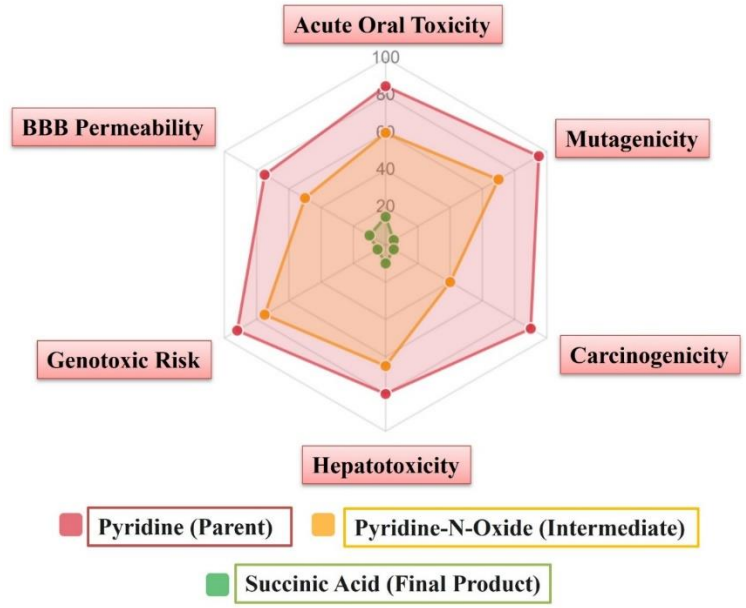

Figure 5. *In silico* comparative toxicity (admet) profile: parent compound (pyridine) vs. primary intermediate (pyridine-n-oxide) vs. final degradation product (succinic acid).

This radar chart (Figure 5) illustrates the progressive reduction in toxicity risk as electrochemical oxidation degrades the parent pyridine compound. The big red zone reflects the high toxicity risk of the parent compound on many parameters. The intermediate (orange) shows less but still notable risk, whereas the ultimate degradation product (green) shows very low toxicity risk, indicating effective detoxification by mineralization.

The Parent Pyridine Derivatives are consistently predicted to be hazardous. As shown in Table 4, compounds like 4-aminopyridine (predicted LD_{50} = 21 mg/kg, WHO Category I) and 2-chloropyridine (LD_{50} = 215 mg/kg, Category II) exhibit high acute oral toxicity. In addition, these parent structures are marked for hepatotoxicity and, importantly, are positive for structural alerts for mutagenicity and carcinogenicity (e.g., pyridine, 2-chloropyridine),

which aligns with their previously noted strong DNA-binding affinity from molecular docking studies.

Primary Degradation Intermediates, such as 2-hydroxypyridine and pyridine-N-oxide, are an important transitional state. Even though they may have lower acute toxicity than their parent (e.g., pyridine-N-oxide LD_{50} = 1500 mg/kg, Category IV), they often include significant risk warnings, those of hepatotoxicity, alongside, in specific cases, mutagenicity. This illustrates that partial degradation reformulates the pollutant into a new, albeit possibly toxic, chemical compound.

The Final Degradation Products - simple aliphatic acids like succinic, maleic, and acetic acid—have very low toxicity. Their calculated LD_{50} values are orders of magnitude greater (e.g., >2000 mg/kg, Category IV), in the low-toxicity range. They are all unanimously calculated to be non-mutagenic, non-carcinogenic, and non-hepatotoxic. Their high renal excretion scores also indicate that they are effectively cleared from the body. Succinic acid, a natural metabolite of the human citric acid cycle, illustrates the innocuous nature of such terminal products.

3.3.3. Integrated toxicity index (ITI) development.

Although molecular docking and ADMET profiling provided essential mechanistic insights into the toxicity of pyridine derivatives and their degradation products, they are static, compound-specific predictions. To supplement these methodologies with a dynamic and system-level analysis, we built an Integrated Toxicity Index (ITI) that calculates the cumulative toxic load of all species present during electrochemical degradation.

The ITI was expressed as:

$$\mathrm{ITI}\ (t) = \sum_i C_i(t) \times \mathrm{TF}_i \qquad (2)$$

Where $C_i(t)$ is the concentration (mg L^{-1}) of species i at time t, calculated from simulated degradation profiles (Table 5), and TFi is its respective toxicity factor. The TFi values were calculated from experimental LD_{50} values (mg kg^{-1}) and binary toxicity indicators (1 for positive, 0 for negative) for mutagenicity (AMES), carcinogenicity (carc), and hepatotoxicity (hepato), as explained in the subsequent weighting scheme:

$$TF_i = \frac{1}{LD_{50}}\left[1+0.2\left(\mathrm{AMES}_{flag}+\mathrm{carc}_{flag}+\mathrm{hepato}_{flag}\right)\right] \qquad (3)$$

Table 5. Calculated toxicity factors (TF) and corresponding input parameters for parent pyridine derivatives and their degradation products used in the Integrated Toxicity Index (ITI) model.

Species	LD_{50} (mg/kg)	AMES	Carc	Hepato	TF
Pyridine	891	1	1	1	2.84
2-Chloropyridine	215	1	1	1	9.90
4-Aminopyridine	21	0	0	1	95.44
Pyridine-N-oxide	1500	1	0	1	1.73
2-Hydroxypyridine	750	0	0	1	2.87
Succinic acid	2260	0	0	0	0.88
Maleic acid	2870	0	0	0	0.70
Oxalic acid	475	0	0	0	4.21

The TF values are based on *in silico* predictions and should be interpreted as relative indicators rather than absolute measures of toxicity.

This expression guarantees that lower LD_{50} (higher acute toxicity) and positive toxicity alerts are given more weight, which represents their higher toxicological significance. The TF values calculated for all species are presented in Table 5.

The development of the ITI during the entire reaction time range is shown in Figure 6a. At t = 0 min, the ITI was characterized by the high levels and high toxicity factors of the parent pyridine bases, namely 4-aminopyridine (very low LD_{50} of 21 mg kg^{-1}, with very high TF = 95.44) and 2-chloropyridine (low LD_{50} and several toxicity flags, TF = 9.90). The electrochemical breakdown proceeded, and the ITI steadily decreased, indicating that these highly toxic parent compounds were degraded rapidly.

At intermediate times (ca. 30-60 min), a short plateau of the ITI degradation was observed. This was attributed to the build-up of toxic intermediates, pyridine-N-oxide (mutagenic and hepatotoxic, TF = 1.73) and 2-hydroxypyridine (hepatotoxic, TF = 2.87). This highlights an important risk of incomplete treatment: partial breakdown can increase or maintain the toxic burden by accumulating bioactive intermediates.

Beyond 90-120 min, the ITI showed a steep and prolonged decrease, corresponding to the ring cleavage of aromatic intermediates and the appearance of terminal aliphatic acids (succinic, maleic, and oxalic acids). These compounds had high LD_{50} values and were free of mutagenicity, carcinogenicity, and hepatotoxicity alerts (except for oxalic acid's moderate acute toxicity, TF = 4.21), contributing appreciably less to the total index. After 180 min of simulated treatment, the ITI decreased to 1.27% of the original value (Figure 6b), clearly establishing successful detoxification through complete mineralization.

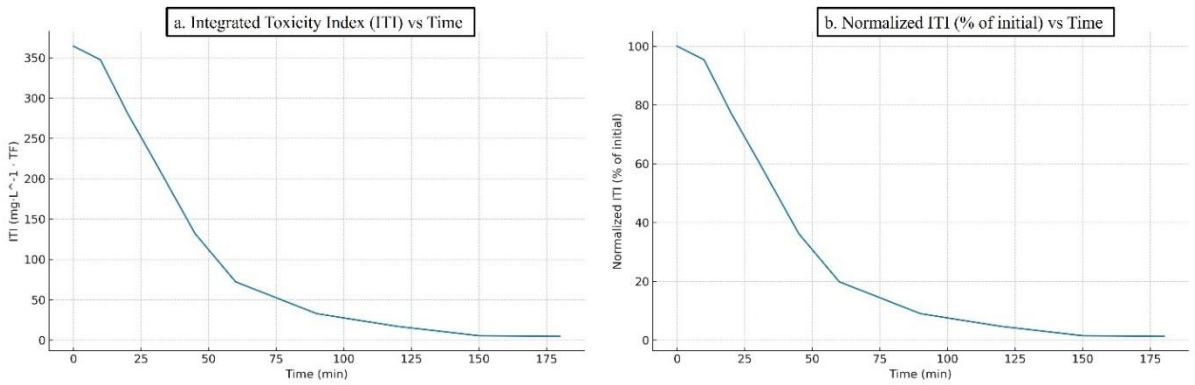

Figure 6. Integrated Toxicity Index (ITI) profiles during electrochemical degradation of pyridine derivatives. **(a)** Evolution over time of the Integrated Toxicity Index (ITI) during the electrochemical degradation process; **(b)** Normalized ITI, as a percentage of the initial value, emphasizing the successful detoxification over time.

To provide a time-integrated measure of toxicity, the area under the curve (AUC) of the ITI profile was calculated. A reduction in AUC reflects a lower cumulative toxic burden over the treatment period. While the observed decrease in AUC supports the trend of diminishing predicted hazard, it should be emphasized that this metric is dependent on modeled concentration profiles and toxicity factors, both of which carry inherent uncertainties.

Furthermore, the above sensitivity analysis indicates that while absolute ITI values vary with changes in weighting factors and input parameters, the overall decreasing trend remains consistent. This suggests that the qualitative conclusion of progressive reduction in predicted hazard is robust, although quantitative values should be interpreted cautiously.

The ITI results are consistent with trends observed in molecular docking and ADMET analyses, in which parent pyridine derivatives generally exhibit higher predicted biological interactions and toxicity alerts than their degradation products. However, it is important to note

that docking scores and ADMET predictions do not directly translate to in vivo toxicity. Therefore, the agreement between these methods and ITI should be considered supportive rather than confirmatory.

3.3.4. Limitations and implications.

The ITI framework provides a useful quantitative tool for comparing toxicity trends during degradation; however, several limitations must be acknowledged: a) ITI relies on predicted or literature-derived toxicity data, which may not fully capture real biological responses. a) Concentration profiles are based on modeled kinetics, not experimental measurements. c) Binary toxicity flags (AMES, carcinogenicity, hepatotoxicity) may oversimplify complex toxicological endpoints.

Therefore, while the results suggest a reduction in predicted hazard during electrochemical degradation, these findings should be validated through experimental toxicological assays and analytical identification of intermediates.

4. Conclusions

This study presents an integrated *in silico* investigation of the electrochemical degradation of pyridine and selected derivatives, combining Density Functional Theory (DFT), reaction pathway modeling, molecular docking, ADMET prediction, and an Integrated Toxicity Index (ITI) framework. The results provide mechanistic insight into degradation pathways, indicating that hydroxyl radical (•OH) attack initiates hydroxylation, followed by ring opening and subsequent oxidation to smaller aliphatic acids. Calculated reaction energetics support the feasibility of these transformation steps and indicate that ring cleavage is a key step in the degradation process.

The ITI analysis, supported by docking and ADMET predictions, indicates a general trend toward reduced predicted hazard as degradation progresses, with parent compounds exhibiting higher toxicity factors compared to most final products. However, intermediate species retained moderate toxicity, highlighting the importance of complete treatment to prevent transient accumulation of potentially harmful compounds.

It is important to emphasize that these findings are based on computational models and predictive tools, which involve inherent uncertainties related to model assumptions, parameter selection, and data sources. Therefore, the results should be interpreted as indicative rather than definitive. In particular, docking scores and ADMET predictions do not directly translate into in vivo toxicity, and the ITI framework serves as a comparative metric rather than an absolute risk assessment.

Future work should focus on experimental validation of the proposed degradation pathways using advanced analytical techniques (e.g., LC–MS/MS) and verification of toxicity reduction through biological assays. Additionally, the influence of operational parameters, such as electrode material, current density, and electrolyte composition, on degradation efficiency and the evolution of toxicity should be systematically investigated.

Overall, this study provides a mechanistic and predictive framework for understanding the degradation and potential toxicity evolution of pyridine compounds during electrochemical treatment, offering a basis for the rational design and optimization of advanced water remediation strategies.

Author Contributions

Conceptualization, all authors; formal analysis, A.K.; writing—original draft preparation, N.C.; supervision, J.K. and A.K. All authors have read and agreed to the published version of the manuscript.

Institutional Review Board Statement

Not applicable.

Informed Consent Statement

Not applicable.

Data Availability Statement

No new data were generated or analyzed in this research. Data sharing is not relevant to this article.

Funding

No external funding was provided for this research.

Acknowledgments

The authors would like to extend their sincere thanks to the Department of Chemistry, School of Sciences, IFTM University, and the MET Faculty of Pharmacy for providing academic and institutional aid.

Conflicts of Interest

The authors have no conflict of interest.

Abbreviations

The following abbreviations are used in this manuscript:

Abbreviation	Definition
ADMET	Absorption, Distribution, Metabolism, Excretion, and Toxicity
AMES	Ames Mutagenicity Test
AUC	Area Under the Curve
BBB	Blood–Brain Barrier
BDD	Boron-Doped Diamond
B3LYP	Becke, 3-Parameter, Lee–Yang–Parr Functional
CO_2	Carbon Dioxide
CYP	Cytochrome P450
CYP2A13	Cytochrome P450 2A13
CYP2E1	Cytochrome P450 2E1
CV	Cyclic Voltammetry
DFT	Density Functional Theory
DNA	Deoxyribonucleic Acid
EAOPs	Electrochemical Advanced Oxidation Processes
EHOMO	Energy of Highest Occupied Molecular Orbital
ELUMO	Energy of Lowest Unoccupied Molecular Orbital
FMO	Frontier Molecular Orbital
GHS	Globally Harmonized System
HClO	Hypochlorous Acid
HOMO	Highest Occupied Molecular Orbital

Abbreviation	Definition
ITI	Integrated Toxicity Index
LC-MS	Liquid Chromatography–Mass Spectrometry
LD_{50}	Median Lethal Dose
LSV	Linear Sweep Voltammetry
LUMO	Lowest Unoccupied Molecular Orbital
MESP	Molecular Electrostatic Potential
NH_4^+	Ammonium Ion
NO_3^-	Nitrate Ion
OH·	Hydroxyl Radical
PDB	Protein Data Bank
pkCSM	Pharmacokinetics of Small Molecules
Pt	Platinum
REACH	Registration, Evaluation, Authorization, and Restriction of Chemicals
TF	Toxicity Factor
Ti/RuO_2	Titanium/Ruthenium Dioxide Electrode
WHO	World Health Organization
AI	Artificial Intelligence
ATP	Adenosine Triphosphate
CI	Confidence Interval
CRISPR	Clustered Regularly Interspaced Short Palindromic Repeats
DNA	Deoxyribonucleic Acid
ELISA	Enzyme-Linked Immunosorbent Assay
GDP	Gross Domestic Product
IRB	Institutional Review Board
LOD	Limit of Detection
MRI	Magnetic Resonance Imaging
PCR	Polymerase Chain Reaction
SEM	Scanning Electron Microscopy
WHO	World Health Organization

References

1. Turovska, B.; Goba, I.; Lielpetere, A.; Glezer, V. Electrochemistry of pyridine derivatives. *J Solid State Electrochem.* **2023**, *27*, 1717–1729, https://doi.org/10.1007/s10008-023-05425-w.
2. Rusu, A.; Moga, I.-M.; Uncu, L.; Hancu, G. The Role of Five-Membered Heterocycles in the Molecular Structure of Antibacterial Drugs Used in Therapy. *Pharmaceutics* **2023**, *15*, 2554, https://doi.org/10.3390/pharmaceutics15112554.
3. Chen, B.; Heal, W. 4.06 - Thiazoles. In Comprehensive Heterocyclic Chemistry III, Katritzky, A.R., Ramsden, C.A., Scriven, E.F.V., Taylor, R.J.K., Eds.; Elsevier: Oxford, **2008**; pp. 635-754, https://doi.org/10.1016/B978-008044992-0.00406-5.
4. Raczuk, E.; Dmochowska, B.; Samaszko-Fiertek, J.; Madaj, J. Different Schiff Bases—Structure, Importance and Classification. *Molecules* **2022**, *27*, 787, https://doi.org/10.3390/molecules27030787.
5. Adesina, A.D. The Chemistry of Benzo and Carbocyclic Derivatives of Pyridine. In Exploring Chemistry with Pyridine Derivatives, Pal, S., Ed.; IntechOpen: London, **2022**, https://doi.org/10.5772/intechopen.108127.
6. De, S.; Ashok Kumar, S.K.; Shah, S.K.; Kazi, S.; Sarkar, N.; Banerjee, S.; Dey, S. Pyridine: the scaffolds with significant clinical diversity. *RSC Adv.* **2022**, *12*, 15385-15406, https://doi.org/10.1039/D2RA01571D.
7. Humans, I.W.G.o.t.E.o.C.R.t. IARC Monographs on the Evaluation of Carcinogenic Risks to Humans. In Some chemicals that cause tumours of the urinary tract in rodents; International Agency for Research on Cancer, **2019**.
8. 7. Humans, I.W.G.o.t.E.o.C.R.t. Pyridine. In Some Industrial Chemicals; International Agency for Research on Cancer, 2000.
9. Ward, E.M.; Schulte, P.A.; Straif, K.; Hopf, N.B.; Caldwell, J.C.; Carreón, T.; DeMarini, D.M.; Fowler, B.A.; Goldstein, B.D.; Hemminki, K.; Hines, C.J.; Pursiainen, K.H.; Kuempel, E.; Lewtas, J.; Lunn, R.M.; Lynge, E.; McElvenny, D.M.; Muhle, H.; Nakajima, T.; Robertson, L.W.; Rothman, N.; Ruder, A.M.; Schubauer-Berigan, M.K.; Siemiatycki, J.; Silverman, D.; Smith, M.T.; Sorahan, T.; Steenland, K.; Stevens, R.G.; Vineis, P.; Zahm, S.H.; Zeise, L.; Cogliano, V.J. Research recommendations for selected

IARC-classified agents. *Environ. Health Perspect.* **2010**, *118*, 1355-1362, https://doi.org/10.1289/ehp.0901828.
10. Časaitė, V.; Stanislauskienė, R.; Vaitekūnas, J.; Tauraitė, D.; Rutkienė, R.; Gasparavičiūtė, R.; Meškys, R. Microbial Degradation of Pyridine: a Complete Pathway in Arthrobacter sp. Strain 68b Deciphered. *Appl. Environ. Microbiol.* **2020**, *86*, e00902-00920, https://doi.org/10.1128/AEM.00902-20.
11. Agency for Toxic Substances and Disease Registry (ATSDR). Toxicological profile for Pyridine. Atlanta, GA: U.S. Department of Health and Human Services, Public Health Service, **1992**.
12. Rodríguez-Peña, M.; Natividad, R.; Barrera-Díaz, C.E.; Balderas Hernández, P.; Alanis Ramírez, C.I.; Roa-Morales, G. Current perspective of advanced electrochemical oxidation processes in wastewater treatment and life cycle analysis. *Int. J. Electrochem. Sci.* **2024**, *19*, 100589, https://doi.org/10.1016/j.ijoes.2024.100589.
13. Yu, J.; Su, N.Q.; Yang, W. Describing Chemical Reactivity with Frontier Molecular Orbitalets. *JACS Au* **2022**, *2*, 1383–1394, https://doi.org/10.1021/jacsau.2c00085.
14. Reddy, P.R.; Prashanth, J.; Prasanna, B.; Reddy, B.V. Synthesis, spectroscopic, and DFT quantum chemical studies of 3- and 4-pyridylacetonitriles. *J. Mol. Struct.* **2019**, *1176*, 447–460, https://doi.org/10.1016/j.molstruc.2018.08.061.
15. Yaqoob, S.; Khan, F.-A.; Tanveer, N.; Ali, S.; Hameed, A.; El-Seedi, H.; Jiang, Z.-H.; Wang, Y. Exploring the Potential of Pyridine Carboxylic Acid Isomers to Discover New Enzyme Inhibitors. *Drug Des. Devel. Ther.* **2025**, *19*, 4039-4091, https://doi.org/10.2147/DDDT.S513461.
16. Karale, R.; Patil, Y.M.; Jahagirdar, S.; Patki, V.; Kulkarni, G. Degradation of personal care product 2-chloropyrine detected in surface water. *Mater. Today Proc.* **2023**, *81*, 137-140, https://doi.org/10.1016/j.matpr.2021.02.820.
17. King, A.M.; Menke, N.B.; Katz, K.D.; Pizon, A.F. 4-Aminopyridine Toxicity: a Case Report and Review of the Literature. *J. Med. Toxicol.* **2012**, *8*, 314–321, https://doi.org/10.1007/s13181-012-0248-9.
18. Hoa, N.T.; Ngoc Van, L.T.; Vo, Q.V. Reactions of nicotine and the hydroxyl radical in the environment: Theoretical insights into the mechanism, kinetics and products. *Chemosphere* **2023**, *314*, 137682, https://doi.org/10.1016/j.chemosphere.2022.137682.
19. Gehring, P.J.; Torkelson, T.R.; Oyen, F. A comparison of the lethality of chlorinated pyridines and a study of the acute toxicity of 2-chloropyridine. *Toxicol. Appl. Pharmacol.* **1967**, *11*, 361–371, https://doi.org/10.1016/0041-008X(67)90079-8.
20. Kaye, A.D.; Coffman, G.D.; Mashaw, S.A.; Thomassen, A.S.; Broocks, K.M.; Anwar, A.I.; Ahmadzadeh, S.; Shekoohi, S. Niacin and Stroke: The Role of Supplementation and Emerging Concepts in Clinical Practice, a Narrative Review. *Curr. Issues Mol. Biol.* **2025**, *47*, 400, https://doi.org/10.3390/cimb47060400.
21. Hejazi, S.A.; Osman, O.I.; Alyoubi, A.O.; Aziz, S.G.; Hilal, R.H. The Thermodynamic and Kinetic Properties of 2-Hydroxypyridine/2-Pyridone Tautomerization: A Theoretical and Computational Revisit. *Int. J. Mol. Sci.* **2016**, *17*, 1893, https://doi.org/10.3390/ijms17111893.
22. Li, D.; Tang, J.; Zhou, X.; Li, J.; Sun, X.; Shen, J.; Wang, L.; Han, W. Electrochemical degradation of pyridine by Ti/SnO_2–Sb tubular porous electrode. *Chemosphere* **2016**, *149*, 49-56, https://doi.org/10.1016/j.chemosphere.2016.01.078.
23. Al Abdel Hamid, A.A.G.; Kanan, S.; Tahat, Z.A. DFT analysis of substituent effects on electron-donating efficacy of pyridine. *Res. Chem. Intermed.* **2015**, *41*, 6859–6875, https://doi.org/10.1007/s11164-014-1783-6.
24. Ruiz-Morales, Y. HOMO−LUMO Gap as an Index of Molecular Size and Structure for Polycyclic Aromatic Hydrocarbons (PAHs) and Asphaltenes: A Theoretical Study. I. *J. Phys. Chem. A* **2002**, *106*, 11283–11308, https://doi.org/10.1021/jp021152e.
25. Naaman, R.; Waldeck, D.H.; Fransson, J. New Perspective on Electron Transfer through Molecules. *J. Phys. Chem. Lett.* **2022**, *13*, 11753–11759, https://doi.org/10.1021/acs.jpclett.2c03141.
26. Jabeen, S.; Khan, M.U.; Ejaz, H.; Waqar, S.; Farhana, A.; Alruwaili, M.; Alruwaili, Y.; Abdalla, A.E.; Mudassar, S.; Ali, Q. Identifying novel inhibitors against drug-resistant mutant CYP-51 *Candida albicans:* A computational study to combat fungal infections. *PLOS ONE* **2025**, *20*, e0318539, https://doi.org/10.1371/journal.pone.0318539.
27. Cuerda-Correa, E.M.; Alexandre-Franco, M.F.; Fernández-González, C. Advanced Oxidation Processes for the Removal of Antibiotics from Water. An Overview. *Water* **2020**, *12*, 102, https://doi.org/10.3390/w12010102.

28. Aarsen, C.V.; Liguori, A.; Mattsson, R.; Sipponen, M.H.; Hakkarainen, M. Designed to Degrade: Tailoring Polyesters for Circularity. *Chem. Rev.* **2024**, *124*, 8473-8515, https://doi.org/10.1021/acs.chemrev.4c00032.
29. Liu, X.; Zhang, X.; Bo, M.; Li, L.; Tian, H.; Nie, Y.; Sun, Y.; Xu, S.; Wang, Y.; Zheng, W.; Sun, C.Q. Coordination-Resolved Electron Spectrometrics. *Chem. Rev.* **2015**, *115*, 6746-6810, https://doi.org/10.1021/cr500651m.
30. Devadiga, D.; Yan, J.; Devadiga, D. Recent Advances in Probing Electron Delocalization in Conjugated Molecules by Attached Infrared Reporter Groups for Energy Conversion and Storage. *ACS Appl. Energy Mater.* **2025**, *8*, 1942–1963, https://doi.org/10.1021/acsaem.4c03246.
31. Singh, A.K.; Bilal, M.; Iqbal, H.M.N.; Raj, A. *In silico* analytical toolset for predictive degradation and toxicity of hazardous pollutants in water sources. *Chemosphere* **2022**, *292*, 133250, https://doi.org/10.1016/j.chemosphere.2021.133250.
32. Brião, G.d.V.; da Costa, T.B.; Antonelli, R.; Costa, J.M. Electrochemical processes for the treatment of contaminant-rich wastewater: A comprehensive review. *Chemosphere* **2024**, *355*, 141884, https://doi.org/10.1016/j.chemosphere.2024.141884.
33. Zhao, M.; Ma, J.; Li, M.; Zhang, Y.; Jiang, B.; Zhao, X.; Huai, C.; Shen, L.; Zhang, N.; He, L.; Qin, S.Cytochrome P450 Enzymes and Drug Metabolism in Humans. *Int. J. Mol. Sci.* **2021**, *22*, 12808, https://doi.org/10.3390/ijms222312808.
34. Guo, Y.; Yue, Q.; Gao, B. Molecular docking study investigating the possible mode of binding of C.I. Acid Red 73 with DNA. *Int. J. Biol. Macromol* **2011**, *49*, 55–61, https://doi.org/10.1016/j.ijbiomac.2011.03.009.
35. Denisov, I.G.; Makris, T.M.; Sligar, S.G.; Schlichting, I. Structure and Chemistry of Cytochrome P450. *Chem. Rev.* **2005**, *105*, 2253–2278, https://doi.org/10.1021/cr0307143.
36. Zanger, U.M.; Schwab, M. Cytochrome P450 enzymes in drug metabolism: Regulation of gene expression, enzyme activities, and impact of genetic variation. *Pharmacol. Ther.* **2013**, *138*, 103–141, https://doi.org/10.1016/j.pharmthera.2012.12.007.
37. Pires, D.E.V.; Blundell, T.L.; Ascher, D.B. pkCSM: Predicting Small-Molecule Pharmacokinetic and Toxicity Properties Using Graph-Based Signatures. *J. Med. Chem.* **2015**, *58*, 4066–4072, https://doi.org/10.1021/acs.jmedchem.5b00104.
38. Daina, A.; Michielin, O.; Zoete, V. SwissADME: a free web tool to evaluate pharmacokinetics, drug-likeness and medicinal chemistry friendliness of small molecules. *Sci. Rep.* **2017**, *7*, 42717, https://doi.org/10.1038/srep42717.
39. Patlewicz, G.; Jeliazkova, N.; Safford, R.J.; Worth, A.P.; Aleksiev, B. An evaluation of the implementation of the Cramer classification scheme in the Toxtree software. *SAR QSAR Environ. Res.* **2008**, *19*, 495–524, https://doi.org/10.1080/10629360802083871.
40. Kumar, A.; Rajput, D.; Gupta, N.; Singh, H.; Chopra, S.; Chopra, H. *In silico* Identification of Promising PDE5 Inhibitors Against Hepatocellular Carcinoma Among Natural Derivatives: A Study Involving Docking and ADMET Analysis. *Drug Res.* **2025**, *75*, 21–33, https://doi.org/10.1055/a-2435-4709.
41. Razaee, Z.S.; Amini, A.A.; Diniz, M.A.; Tighiouart, M.; Yothers, G.; Rogatko, A. On the properties of the toxicity index and its statistical efficiency. *Stat. Med.* **2021**, *40*, 1535–1552, https://doi.org/10.1002/sim.8858.
42. Hays, R.D.; Ganz, P.A.; Spritzer, K.L.; Rogatko, A. Applying the Toxicity Index to Patient-Reported Symptom Data: An Example Using the European Organization for Research and Treatment of Cancer Colorectal Cancer–Specific Quality of Life Questionnaire. *Clin. Ther.* **2021**, *43*, 1245–1252, https://doi.org/10.1016/j.clinthera.2021.05.011.
43. Macchia, A.; Valentini, F.; Colasanti, I.A.; Zaratti, C. Prediction of Green Solvent Applicability in Cultural Heritage Using Hansen Solubility Parameters, Cremonesi Method and Integrated Toxicity Index. *Sustainability* **2025**, *17*, 2944, https://doi.org/10.3390/su17072944.
44. Morroni, L.; Pinsino, A.; Pellegrini, D.; Regoli, F.; Matranga, V. Development of a new integrative toxicity index based on an improvement of the sea urchin embryo toxicity test. *Ecotoxicol. Environ. Saf.* **2016**, *123*, 2–7, https://doi.org/10.1016/j.ecoenv.2015.09.026.

Publisher's Note & Disclaimer